Environmentally Friendly Low Temperature Solid State Micro-joining

TAKAHASHI Yasuo* and MAEDA Masakatsu**

Abstract

The present review describes the low temperature solid state micro-joining applied to advanced electronics packaging. Four topics are introduced. The first one concerns the trend of semi-conductor packaging. The second one is the room temperature bonding carried out under an ultra high vacuum condition. The third one is the mechanism of micro bump bonding applied to the electronic assemblies. The bump bonding is usually called "flip chip bonding (FCP)" and is applied to the chip scale packaging (CSP), which is very important for three dimensional packaging. The bump deformation behavior is visualized by numerical simulation. The bond area growth mechanism (slip and folding mechanism) is numerically analyzed. The last one is the ultrasonic bonding between Au wire and Al pad. The Al pad has a very strong thin oxide film on the surface. The breakdown of the oxide film is discussed based on the idea of the slip and folding mechanism. The effect of ultrasonic vibration on the low temperature solid state micro-joining process is also discussed.

KEY WORDS: (Room temperature bonding) (Micro-joining) (Flip chip bonding) (Chip scale packaging) (Ultrasonic bonding) (Solid state joining) (Environmentally benign technology) (Eco technology) (Electronic assembly)

1. Introduction

The solid state technology such as low temperature micro-joining is very important for electronic assembly technology [1, 2, 3]. Solid state micro-joining is one of the environmentally benign technologies, because it is essentially a low temperature process and it needs no filler metals[1, 4]. The solid state joining is also indispensable for nano- and micro-scale material processing and three dimensional (3D) electronic assembly technology [5]. The present review, therefore, describes the trends of semi-conductor packaging and the solid state micro-bonding mechanisms. The three kinds of joining technology are introduced; surface activated room temperature bonding, flip chip bonding (fine bump bonding) and ultrasonic wire bonding.

2. Environmentally benign electronics packaging

In recent years, ECO (Environmentally Conscious) -design, -production and -manufacturing became necessary in all companies, based on WEEE, RoHS, and the ISO 14000 series restriction from the view point of CSR (Corporate Social Responsibility). However, for commodities such as electrical appliances and vehicles, the waste energy and garbage disposal from the consumers (end users) give the global environment more burden than the manufacturing processes. Thus, energy saving or high energy efficiency in using the commodities have to be taken into consideration in the manufacturing and joining processes. In electronics packaging, the chip scale packaging (CSP) and 3D assembly became necessary to increase the energy saving and data memory capacity. So, the size of micro-joining must be decreasing as indicated in **Fig. 1**. The tertiary revolution is now done, for example, the system in packaging (SiP) and Chip on Chip (CoC) assembly have been developed as illustrated in Fig. 1. As several chips have to be stacked in SiP as illustrated in Fig. 1, a lot of interconnections are necessary. The flip chip bonding and gang connection processes are indispensable for high density

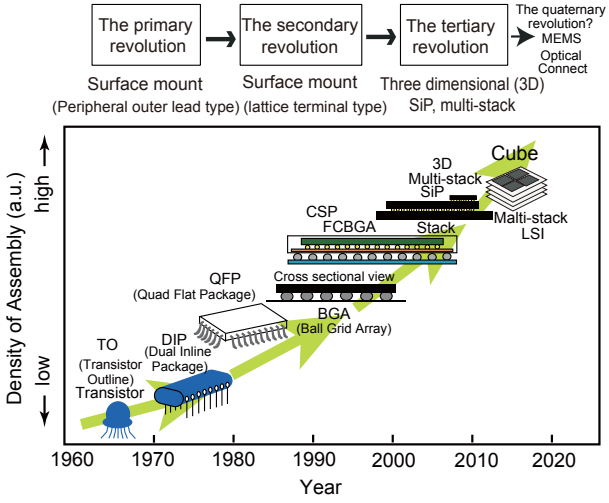

Fig. 1 Trend of electronics packaging technologies.

* Professor, JWRI, Osaka University
** Assistant Professor, JWRI, Osaka University

Transaction of JWRI is published by Joining and Welding Research Institute of Osaka University, Ibaraki, Osaka 567-0047, Japan

Table 1 Flip chip bonding and gang connection for high density packaging.

Phase and direction to low temp.	Liquidus ← Low temperature → Solidus							
Bonding Mechanisms, etc	Soldering Wetting		Wetting and interface-reaction	Resin Adhesive ACF/ACP	Resin Adhesive NCF/NCP	Slip and folding	Plating	Elasto-plastic contacting
Structure	IC chip / Substrate							
Bump materials	C4: Pb solder	C2: Metal(Cu) + Pb free Solder	Au bump Stad	ex. Au bump Stad	ex. Au bump Stad	Au bump Stad	No bumps	Adhesive (resin) Au bump
land or pad of substrate	Pre-solder	Anti-rust	Pre-solder	Au plating	Au plating	Au electrode	Cu pads	Bump flattening by cuting
Connection materials	Solder	Solder	Low temp. Solder	Micro metal particle/Au	Au/Au	Au/Au	Ni-B/Cu	Au/Au
Connection methods	Reflow	Reflow	Reflow or TCB	TCB	TCB	TSB	Electroless plating	Au/Au contact and Adhesion

Note C4 : Controlled collapse chip connection, C2 : Chip connection, ACF/ACP : Anisotropic conductive film/paste, NCF/NCP : Non conductive film/paste
TCB : Thermo-compression bonding, TSB : Thermosonic bonding,

packaging. The interconnection types used in the flip chip bonding are arranged in **Table 1**. As seen in the left hand side of Table 1, liquid phase such as soldering is used. But solidus phase is applied to FCB if we wish to decrease the process temperature, as seen in the right hand side of Table 1. It is suggested that the solidus phase is more suitable for high density packaging although soldering (reflow) is of lower cost. Resin adhesive is also a low temperature process with low cost and many kinds of adhesive process (ACF/SCP, NCF/NCP, referred in Table 1) have been developed. The room temperature bonding of Au/Au bumps is applied to FCB. In the next session, the fundamental study of surface activated room temperature micro bonding between Au fine wires and Au flat foils (electronic pads) is reviewed.

3. Surface activated room temperature bonding

Surfaces of materials exposed in air are usually covered with oxide film or contamination. It is therefore not easy to bond them in air under pressureless and heatless conditions. However, if the oxide film and contamination are removed by ion or atom irradiation and the surface is activated, then the adhesion can be produced at room temperature and lowest pressure conditions. As the size (radius) of wire and bump (sphere) decreases, the effect of surface energy becomes very important, i.e., the surface energy should be taken into consideration for elastic adhesion. The nano and/or micro adhesional bonding becomes possible [6].

Fig. 2 shows a comparison between the experimental half bond width a and the calculated results of half theoretical adhesional contact width a_j, half the elasto-plastic adhesional contact width a_{ep} and half the plastic adhesion width a_p for Au fine wire (the radius: R = 50 μm)-Au foil (thickness: 130 μm). The bonding temperature T is 298 K. Bonding time t_B (the duration when the pressure is applied to the wire) is 60 s. The experimental procedure has been explained elsewhere [7]. Atmospheric condition (vacuum degree) for bonding was about 1.5×10^{-8} Pa. The bonding surfaces were cleaned by argon ion irradiation before bonding. As seen in Fig. 2, the experimental bond width a is always larger than the value of a_j and is good agreement with a_{ep}. The ductile separation of the junction was observed under $P > 2$ MPa, where P is the applied mean pressure, i.e., $P = f/2R$, where f is the applied force per unit length of wire and R is the wire radius. The range of P = 2~20 MPa corresponds to the transition region from elastic to plastic contact, i.e., elasto-plastic contact is produced. The perfect plastic contact occurs in the range of $P > 20$ MPa. If the pressure is low enough to produce the elastic

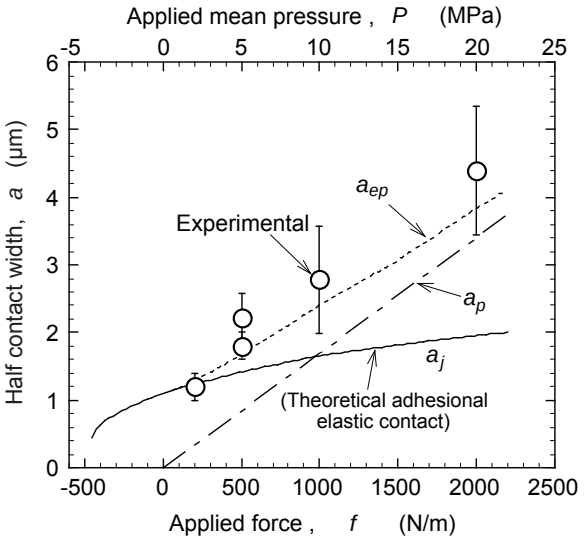

Fig. 2 Comparison between calculated results (a_j, a_{ep}, and a_p) and experimental results (white circles) for Au wire-Au foil. The bonding was carried out at 298 K. The pressure was applied for 60 s.

adhesion partially, the bond strength gradually increases with increasing the holding (aging) time after bonding [8]. Elastic internal stress usually exists as a residual stress around the elastic contact between wire and foil [8]. The elastic stress distribution allows a vacancy diffusion along the adhesional contact interface.

Fig. 3 shows the change in the bond strength per unit bonded area $\sigma_p = F_p/A_c$, where F_p is the pull strength and A_c is the contour area bonded. The plots of σ_p - $t^{1/2}$ exhibit a linear relationship. This is due to the stress induced diffusion which must occur along the bond interface [8].

Fig. 4 shows the change in the bonded area A_c with the holding time t_r after bonding. The temperature T shown in Fig. 4 is the holding temperature after bonding. All bonding tests were carried out at the room temperature (298 K). As seen in Fig. 4, the bonded area scarcely increases with the holding time t_r. The experimental points of (a)~(e) in Fig. 4 corresponds to those of Fig. 3. The temperature dependence of the change in σ_p

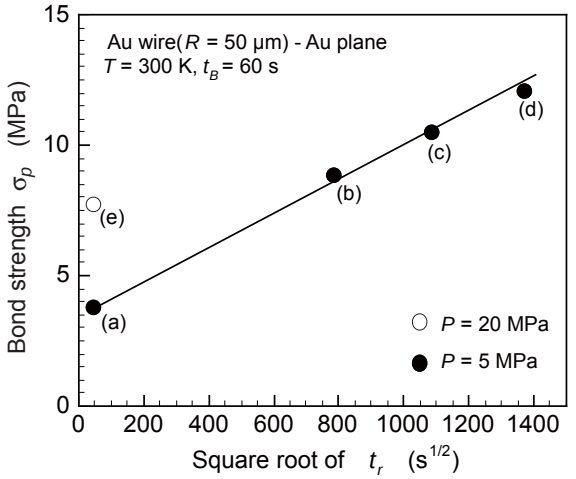

Fig. 3 Change in bond strength with holding time after bonding. The bond-strength σ_p was obtained by pull strength F_p divided by the bonded area (contour area).

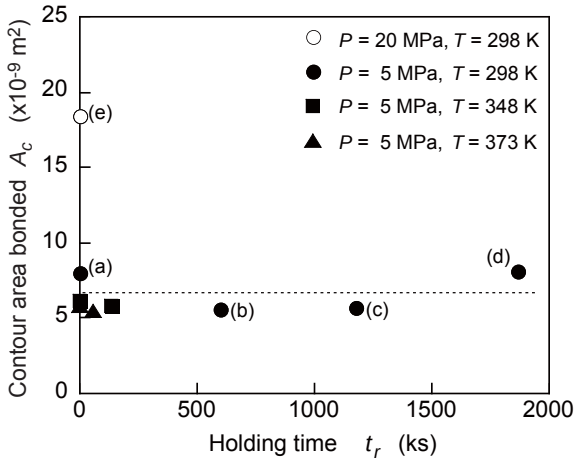

Fig. 4 T/t_r-$1/T$ plots. The experimental points (a)~(e) corresponds to those of Fig. 3.

with t_r was investigated [8]. As a result, the increase in the bond strength becomes striking with increasing the holding temperature T after bonding.

As described above, the elastic adhesional contact produces local residual stress (tensile stress) around the bonded interface. The increase in the bond strength is, therefore, due to the stress relaxation by the stress induced vacancy diffusion [8]. Because of low temperatures (annealing temperature T = 298~373K), the vacancy diffusion along the bonded interface can govern the stress relaxation process [7, 8]. This was verified by T/t_r-$1/T$ plots, where t_r is the time taken to obtain certain increase in the bond strength (for example, the time required to obtain the strength of F_p = 45 mN as reported in [8]). The value of T/t_r is proportional to $D_{bo}\exp(-Q_b/RT)$, where D_{bo} is the frequency factor of grain boundary (or interface) self-diffusion, Q_b is the activation energy and R is the gas constant. In fact, the activation energy (76.0kJ/mol) was obtained from the experimental results (T/t_r-$1/T$ plots). The value of 76.6 kJ/mol was somewhat less than that of the grain boundary self-diffusion of Au (87 kJ/mol). The activation energy of vacancy diffusion consists of Q_f and Q_m, where Q_f is the formation energy of a vacancy and Q_m is the migration energy. The surface activation process of Ar ion irradiation before bonding can increase the vacancy concentration around the bonding surface, resulting in the decrease of Q_f. This is the reason why Q is less than Q_b [8].

The adhesion behavior also depends on replacing the materials of wire and foil. The contact width becomes larger when softer metal is used as a foil. In the adhesion between Al wire and hard foils (Au, Ni or Cu) , the adhesion is easily formed at the periphery of contact area. On the other hand, the adhesion between Al foil and hard wires is easily formed in the central area [9]. The reason is the difference in elasto-plastic deformation pattern of wire and foil. Also, the effective yield stress can change between the couple of wire and pad. In the room temperature bonding of dissimilar metals and dissimilar shape (wire and foil), we can often observe very interesting phenomena.

4. Micro-bump bonding

Chip scale packaging (CSP) is necessary for the high density electronic assembly and will be indispensable for the next generation interconnection technologies. The flip chip bonding (FCB) has been applied to the inter-connection between IC chip and the electronic circuit on substrates as shown in Fig.1. Solid state bonding is very often used for CSP. For example, thermosonic Au bump bonding to Al electric pad (or Au land) has been used as FCB.

In this session, the ultrasonic bump bonding is discussed as an example of micro-bump bonding technologies. An ultrasonic vibration is applied to the bonding interface parallel to the bonding interface together with the bonding pressure (load). The ultrasonic vibration facilitates the frictional slip and the plastic deformation but the effect of ultrasonic vibration on the bonding process is not clearly understood. It is very important to understand the interfacial behavior during the bump bonding but experimental visualization of the interfacial behavior is very difficult. Numerical studies of inner lead bonding and wire bonding [10, 11] have been carried out but there are few numerical studies of the ultrasonic bump bonding. Therefore, in the present review, numerical modeling and simulation of thermosonic bump bonding is introduced.

Fig. 5 illustrates a two dimensional finite element model of the micro bump bonding. Fig. 5 (a) is for a barrel type bump and Fig. 5 (b) is for a bowl type bump in order to compare the difference of deformation pattern between the barrel type and the bowl type bumps. Mesh patterns of the finite element model (FEM) used in the present study are illustrated. Also, the inset figure of Fig. 5 shows the ultrasonic vibration wave pattern and the time steps of 1~9. The time increment Δt was 1/8 of the period. The wave pattern (frequency f_v and amplitude A_o) is assumed to be very simple and constant during bonding in numerical simulation, although it usually changes in the actual bonding. It is assumed that the gold bump surface and the gold pad surface slide and are bonded with each other. It is assumed that the ultrasonic vibration amplitude A_o is small enough so that the each nodal point cannot slip largely for the time increment Δt , i.e., the slip model can treat only the micro (nano)-slip, the direction of which rapidly changes, following the ultrasonic vibration. The frictional slip occurs when $|\tau_{xy}| > \mu|\sigma_y|$, where μ is the friction coefficient, τ_{xy} is the shear stress, and σ_y is the stress in the y direction in Fig. 5. It is hard task to solve the slip rate in self-consistency at each step so that the relation of $|\tau_{xy}| \approx \mu|\sigma_y|$ can be satisfied. The stress distribution at the next step is accommodated by the micro frictional slip. The frictional slip model should not be applied to the large slip behavior, because the stress relaxation at each step is not satisfied [1]. This assumption is not adequate for Al wire bonding because the large frictional slip is necessary for the central area bonding between Al wire and Al pad. Bump deformation process and interfacial micro slip behavior during flip chip bonding were simulated by the FEM, in which the stress dependence of strain rate was taken into account [1, 10, 11].

Fig. 6 shows the equivalent stress distributions during barrel type bump bonding (f_v = 60 kHz). Fig. 6 (a) is for thermocompression bonding without ultrasonic vibration. The maximum stress level is not more than 200 MPa. Fig. 6 (b) is for thermosonic bonding with ultrasonic vibration. The maximum stress value is much greater than the applied pressure P = 196 MPa. As seen

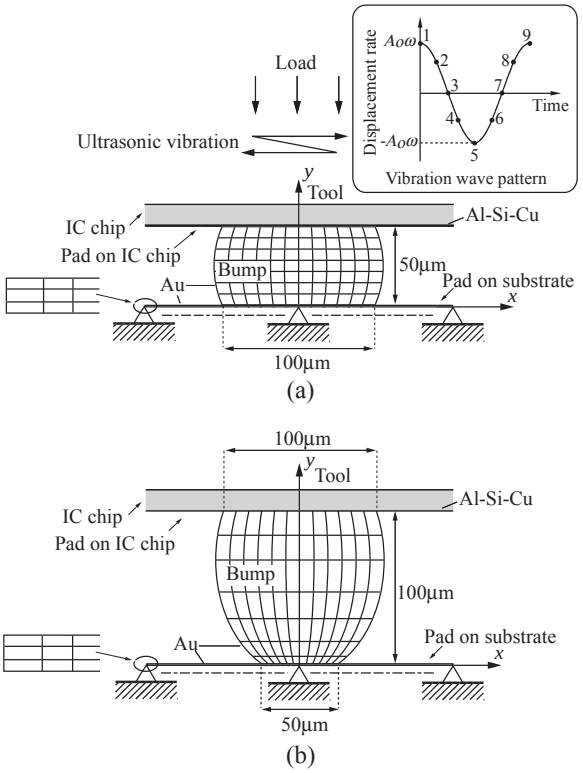

Fig. 5 Two dimensional models of Au bump bonding. (a) barrel type bump and (b) bowl type bump.

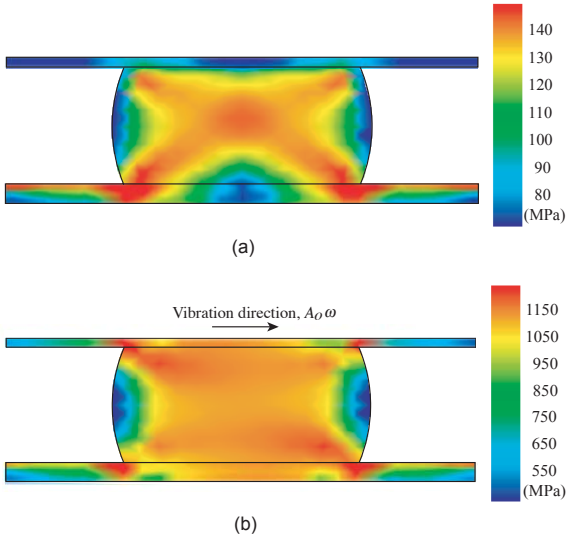

Fig. 6 Distribution of equivalent stress at t = 1.67 x 10^{-5} s (T = 473 K, P = 196 MPa).
(a) TC (thermocompression) bonding,
(b) US (ultrasonic) bonding (A_o = 50 nm, f_v = 60 kHz).

in Fig. 6, the maximum stress value in Fig. 6 (b) is 10 times greater than that of Fig. 6 (a). The ultrasonic vibration largely enhances the equivalent stress of the driving force for visco-plastic deformation. So, the bump deformation is facilitated by the ultrasonic vibration. The stress distribution changes on the bond interface with ultrasonic vibration. The micro frictional slip is not uniform. The numerical results suggest that the stress in the *y* direction changes from compressive to tensile at the edge of the bond-interface, synchronizing with the ultrasonic vibration, when the slip is micro and nano level. On the other hand, if a large gross slip occurs, then the stress relaxation is produced and the plastic deformation of bump cannot be facilitated, i.e., if the substrate begins to oscillate simultaneously with the bump side, the facilitation effect is reduced. At that stage, the stress distribution will be very different from the case when the micro slip just occurs. In other words, there is an important problem on the assumption of the boundary condition which is given to the bonding interface. It is very difficult to give an adequate boundary condition

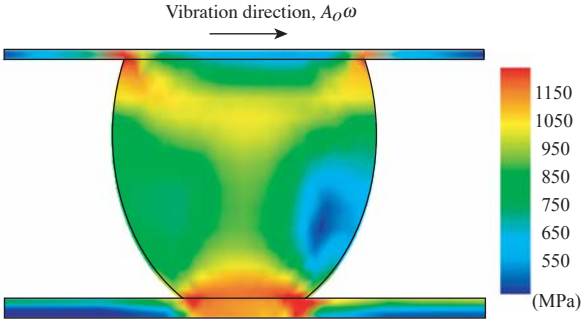

Fig. 7 Equivalent stress distribution of bowl bump (t =1.67x10^{-5} s). P = 196 MPa, T = 473 K with US vibration (A_o = 50nm, f_v = 60 kHz).

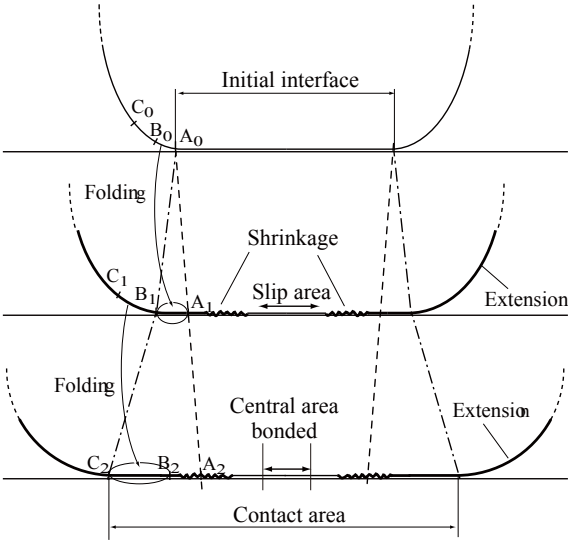

Fig. 8 Schematic illustration of slip and folding mechanism.

to the bonding interface when the adhesion phenomena occurs on the bonding interface. This is the true nature of the problem when we discuss the joining science.

Fig. 7 shows the equivalent stress distribution during bowl bump bonding. This result is also for the case when the micro slip just occurs. The stress increases at the bond interface. The high stress concentration produces the folding phenomena so that the bump side surface touches the pad surface, resulting in the bonded area growth. Under the condition of the micro-slip assumed in this numerical simulation, the micro-slip easily occurs in the early stage of bonding and in the central contact area. It is suggested from the numerical simulation that the slipped area (bump side) shrinks and adheres and the periphery (bump surface) area is folded to the pad surface. Let us define this as the slip and folding mechanism, which is illustrated in **Fig. 8**.

In Fig. 8, the frictional micro-slip occurs at the initial contact area. The slipped area shrinks because the normal stress becomes larger in front of the slip direction, reducing the front area slip. If the central area frictionally slides, the oxide film is broken and the friction coefficient is increased, i.e., the central area adheres.

The equivalent stress is enhanced by the ultrasonic power, if the central area is fixed. As a result, the bump easily deforms and the folding phenomena is produced. The slip and folding repeatedly occurs, synchronizing with the ultrasonic vibration. This is the slip and folding mechanism. Immediately after the bump surface folding, the new interface slips and adheres. After that, the bump surface is folded to the new pad surface and the bonded area spreads by repeat of slip and folding. The bonded area growth is not produced by expansion (extension) of the initial bond-interface. The slip and folding mechanism is the dominant mechanism which increases the bond area in the bump bonding. The slip and folding mechanism can also govern the wire bonding.

5. Fine wire bonding

The wire bonding mechanism has not perfectly been solved yet. It is very important to clarify the wire bonding mechanism for developing the next generation interconnection technology. Therefore, in the present review, the bonding mechanism is discussed. The actual thermocompression bonds or thermosonic bonds often exhibit the perimeter bond formation as the bonding load increases, i.e., a doughnut configuration (periphery area bonded and no bonds in the central area) are sometimes observed under high pressure conditions.

Fig. 9 shows the experimental results of ball bonding of Au wire. The diameter of the wire is 25 μm. The Au ball was bonded to Al (-Si-Cu) pad with the thickness

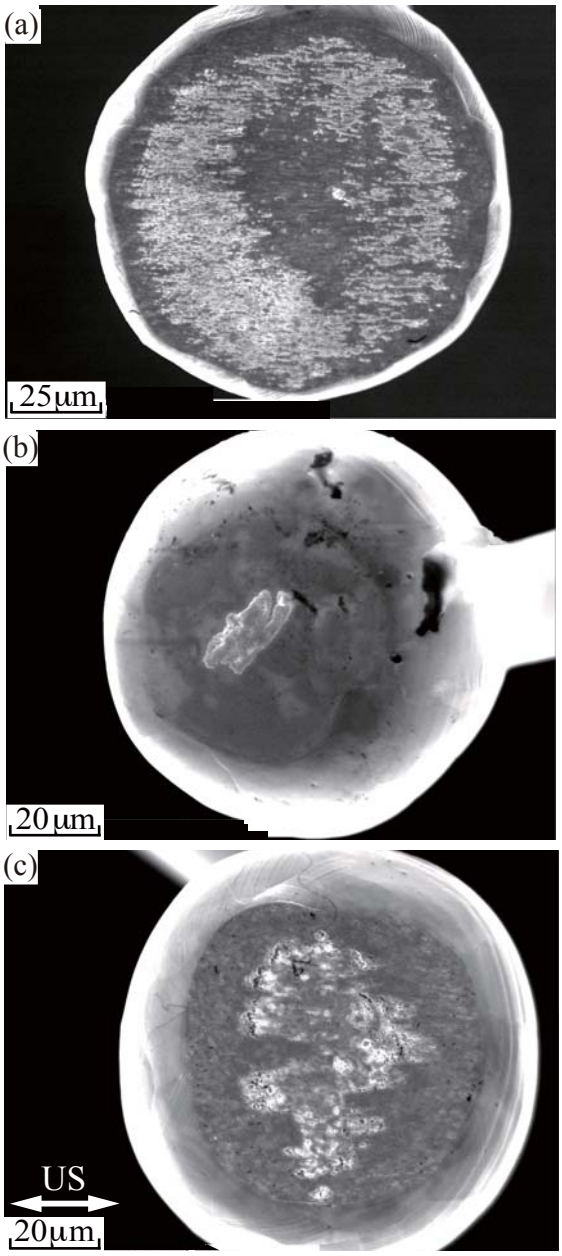

Fig. 9 Au-Al intermetallic compound on ball surface after wire bonding (SEM).
(a) T_{stage} = 523 K, F_{WB} = 0.95 N, t = 200 ms, ΔH / H_0 = 66.9 %,
(b) T_{stage} = 353 K, F_{WB} = 0.50 N, W_{US} = 20 mW, t = 20 ms, ΔH / H_0 = 24.3 %
(c) T_{stage} = 353 K, F_{WB} = 0.50 N, W_{US} = 20 mW, t = 80 ms, ΔH / H_0 = 42.3 %, where ΔH is the reduction of Au wire ball and H_o is the initial mean height of the wire ball (nearly equal to the wire ball diameter). $\Delta H/H_o$ is defined as the compression ratio.

of 1 μm. SEM (scanning electron microscopic) photos were taken after the wire was removed from Al pad by 10% dilute hydrochloric acid. Therefore, the white area in the photos indicates the intermetallic compounds between Au and Al which were formed during the bonding process. The stage temperature T_{stage}, the bonding force F_{WB} and the ultrasonic power W_{US} were changed as shown in the caption of Fig. 9. If W_{US} = 0 (the thermo-compression condition of Fig. 9 (a)) and the temperature is high (T_{stage} = 523 K), the central area is not bonded as seen in Fig. 9 (a). The oxide film of Al pad is not broken down by the ultrasonic vibration. On the other hand, if the ultrasonic power (f_v = 60 kHz) is applied and the bonding force is not so high, then the bonding (adhesion) begins from the central area as can be seen in Fig. 9 (b). By increasing the bonding time t, the compression ratio $\Delta H/H_o$ increases, the wire ball largely deforms, and the bonded area increases as seen in Fig. 9 (c). This is driven by the slip and folding mechanism shown in Fig. 8. When the slip and folding mechanism work well, the surface oxide film can be broken by the frictional slip. The oxide film behavior was investigated during Al wedge bonding [12]. The TEM observation is very significant in understanding the breakdown process of the oxide film.

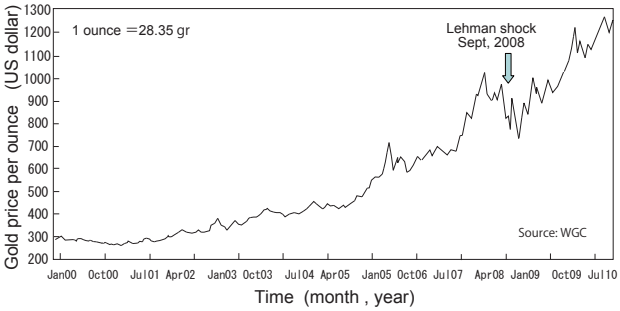

Fig. 10 Transition of the gold price (per ounce) in the London market.

Fig. 10 shows the transition of the gold price (per ounce) in the London market. Recently, the price of gold has being increasing from 2000 although it decreased once at the Lehman shock. This rise gave us a driving force to the process change from Au wire to Al or Cu wires the cost of which are lower than that of Au. Cu wire or ribbon bonding are becoming important processes [13, 14]. Cu wire and ribbon bonding is not an easy technology because Cu is harder than Au and Al and Cu surface is unstable and gradually oxidized. It is very important to understand the slip and folding mechanism for Cu bonding. It is indispensable to bear environmentally benign joining processing in mind.

6. Conclusive remarks

The solid state technology is indispensable for the next generation 3D interconnection. It is important to understand the solid state micro-bonding mechanisms. In the present review, trend of semiconductor package

was simply explained. Also, the surface activated room temperature bonding under ultra high vacuum condition, the micro-bump bonding and fine wire bonding were discussed. In the room temperature bonding, it was found that the bond strength gradually increases with time after bonding. The cause is the stress induced vacancy diffusion (along the bonded interface if the holding temperature is low enough) which reduces the tensile stress due to adhesional elastic contact. In the micro-bump bonding, it was suggested that the slip and folding mechanism controlled the bonding process. The frictional slip is not uniform and the slipped area tends to shrink. In the fine wire bonding, it was described that the slip and folding mechanism governs the wire bonding. These phenomena should be understood when developing the new solid state bonding.

References

1) Y. Takahashi, "Future Direction of Solid State Mcro-joining Applied to Environmentally Friendly Electronic Packaging, " The IECE Trans. on Elec tronics, The institute of Electro. Infor. Communi. Eng., Vol. J92-C, No.11 (2009) pp.581-594 (in Japanese).
2) Y. Takahashi and M. Maeda, "Advanced Eco Electronics Packaging and Low Temperature Bonding," MATE 2011, JWS, Vol. 16 (2010) pp.389-392.
3) Y. Takahashi, "Trend of Electronics Assembly Tecnology as Torchbearer of 21 Century Environmental Revolution," J. High Temp. Society, Japan, Vol. 30, No. 1 (2004) pp.16-23.
4) Y. Takahashi and M. Maeda, "Application of Solid State Bonding to Manufacturing Eco Products,"Smart Processing Technology, Vol. 1 (2006), High temp. Soc. Japan, pp. 163-166.
5) T. Suga and K. Otsuka, "Bump-less Interconnect for Next Generation System Packaging," Electronic Components and Technology Conference (ECTC), (2001) Doc. 0-7803-7038-4.
6) Y. Takahashi, "Adherence of Fine Wire---Solution by Energy Minimum Principle and Nano Adhesional Bonding---," Trans. JWRI, Vol. 30 (2001)pp.23-31.
7) Y. Takahashi and S. Matsusaka; "Adhesional Bonding of Fine Gold Wires to Metal Substrates," J. Adhesion Sci. Technol. Vol. 17, No.3 (2003) pp. 435-451.
8) Y. Takahashi and K. Uesugi, "Stress Indued Diffsion along Adhesional Contact Interfaces," Acta Materialia, Vol. 51 (2003) pp. 2219-2234.
9) Y. Takahashi M. Maeda, T. Doki and S. Matsusaka, "Room Temperature Micro-bonding of Fine Wires to Foils," Solid State Phenomena, Vol. 127 (2007) pp. 277-282.
10) Y. Takahashi, M. Inoue and K. Inoue, "Numercal Analysis of Fine Lead Bonding --- Effect of Pad Mechanical Properties on Interfacial Deformtion---," IEEE Trans. Comp. Pack. Technol., Vol. 22 (1999) pp. 558-566.
11) Y. Takahashi and M. Inoue, "Numerical Study of Wire Bonding ---Analysis of Interfacial Deformtion Between Wire and Pad," J. Electronic Pack. ASME, Vol. 124 (2002) pp. 27-36.
12) S. Kitamori, M. Maeda and Y. Takahashi, "Interfcial Microstructure between Thick Aluminum Wire and Pad Formed by Ultrasonic Bonding," MATE 2006, Yokohama, 2-3, Feb. (2006), JWS, pp. 345-348.
13) Tian Yan-hong, Wang Chun-qiung, Y. N. Zhou, "Bonding mechanism of ultrasonic wedge bonding of copper wire on Au/Ni/Cu substrate," Trans. No-ferrous Met. Soc. China, Vol. 18 (2008) pp. 132-137.
14) M. Maeda, T. Sato, N. Inoue, D. Yagi and Y. Takahashi, "Anomalous microstructure formed at the interface between copper ribbon and tin-deposited copper plate by ultrasonic bonding," Microelectronics Reliability, Vol. 51 (2011) pp. 130-136.